Journal of Power Sources 199 (2012) 402–408

Contents lists available at SciVerse ScienceDirect

Journal of Power Sources

journal homepage: www.elsevier.com/locate/jpowsour

The effects of surfactant template concentration on the supercapacitive behaviors of hierarchically porous carbons

Xiaoyan Zhang, Xianyou Wang*, Jinchang Su, Xingyan Wang, Lanlan Jiang, Hao Wu, Chun Wu

Key Laboratory of Environmentally Friendly Chemistry and Applications of Minister of Education, School of Chemistry, Xiangtan University, Hunan, Xiangtan 411105, China

ARTICLE INFO

Article history:
Received 7 August 2011
Accepted 17 October 2011
Available online 20 October 2011

Keywords:
Hierarchically porous carbon
Surfactant
Supercapacitor
Electrochemical performances

ABSTRACT

The hierarchically porous carbons (HPCs) are prepared by sol–gel self-assembly technology at various surfactant concentrations (from 0 to 0.55 mol L^{-1}). The influences of the surfactant (CTAB) concentration on the physical and electrochemical properties of the activated HPCs are investigated by nitrogen adsorption–desorption isotherm, cyclic voltammetry, galvanostatic charge–discharge, cycle life, electrochemical impedance spectroscopy (EIS) and self-discharging in 6 M KOH electrolyte. The results demonstrate that the concentration of surfactant template is a crucial factor impacting the characteristics of HPCs. With the change of surfactant concentration, the activated HPCs at C_{CTAB} = 0.27 mol L^{-1} (HPCs-3) shows the largest specific surface area of 689 m^2 g^{-1}. In addition, the activated HPCs show excellent supercapacitive behaviors and three sections self-discharge mechanism. Especially, the activated HPCs-3 appears superior electrochemical stability, low IR drop of 0.01 V, and the maximum specific capacitance of 272 F g^{-1} obtained from cyclic voltammetry at the scan rate of 1 mV s^{-1}. Moreover, the supercapacitor used the activated HPCs-3 as electrode active material exhibits a specific capacitance of 61 F g^{-1} at the current density of 1 A g^{-1}, and keeps a specific capacitance of 60 F g^{-1} after 5000 consecutive charge/discharge cycles.

1. Introduction

Electrical double layer capacitors (EDLCs) have gained a significant amount of interest and attention because they deliver high power and store conspicuous energy. Being charged/discharged for thousands of cycles with little influence of cycle-life, good conductivity and low cost, EDLCs have been extensively applied to many fields such as mobile phones, laptops, radio tuners, digital camera, EV and HEV.

It is well known that the key of development of EDLCs depends upon the development of the electrode material with high performance. Currently, the electrode materials for the application of EDLCs are activated carbons (ACs) [1], carbon nanotubes (CNTs) [2], carbon nanofibres (CNFs) [3], carbide-derived carbons (CDCs) [4] and template-derived carbons (TDCs) [5]. Among above carbon materials, TDCs have drawn much attention as they provide high specific surface area with regularly interconnected pores that allow for improving ionic transport and power density. Nowadays, template-derived carbons with highly porous structures are prepared by filling porous structure of an inorganic matrix with a carbon precursor, e.g., sucrose, propylene, pitch or polymer solutions [6–9]. Template-derived carbons with varying ordered pore symmetries and mesopore structure have been prepared by Xing et al. [10]. The specific capacitance is about 220 F g^{-1} with surface areas of 1500–1600 m^2 g^{-1}. In order to further improve their capacitive performance, some studies have focused on making use of modified templates to prepare hierarchically porous carbons (HPCs) [11–13]. It is deliberately designed to obtain a micropore structure existing in hierarchically porous carbons, in which the macropores can form ion-buffering reservoirs, and the mesopores provide a short ion-transport pathway while the micropores may strengthen the electrical double-layer capacitance [14,15]. Wang et al. [14] reported the electrochemical performance of three-dimensional (3D) aperiodic hierarchical porous graphitic carbon, and discovered that the hierarchical porous texture composed of macropores, mesopores and micropores displayed a great potential for advanced electrochemical capacitor applications. However, it is quite rarely reported about the effects of the surfactant template concentration on the pore structure and electrochemical performance of HPCs.

Recently, our group has carried out a lot of researches on porous structure carbon materials and their supercapacitive behaviors. In this paper, hierarchically porous carbons (HPCs) with micro–meso–macro structures are prepared by sol–gel self-assembly process, herein the surfactant (cetyltrimethyl ammonium bromide, CTAB) and nickel oxide are used as dual templates and the phenolic resin is used as the carbon sources. In order to further improve their performance, the as-prepared HPCs are activated by

* Corresponding author. Tel.: +86 731 58292060; fax: +86 732 58292061.
E-mail address: wxianyou@yahoo.com (X. Wang).

0378-7753/$ – see front matter © 2011 Elsevier B.V. All rights reserved.
doi:10.1016/j.jpowsour.2011.10.070

2 M HNO_3. The effects of the surfactant template concentration on physical and electrochemical properties of hierarchically porous carbons are studied in detail.

2. Experimental

2.1. Synthesis of the activated HPCs

Hierarchically porous carbons were prepared by carbonization and corrosion of the dual template precursor. Nickel nitrate hexahydrate ($Ni(NO_3)_2{\cdot}6H_2O$, 98%) and sodium hydroxide (NaOH, 96%) were used as nickel oxide template, and cetyltrimethyl ammonium bromide (CTAB, 99%) dissolved in ethanol-aqueous solutions was used as the surfactant template. The molar ratios of $Ni(NO_3)_2$ and CTAB were 4:0, 4:2, 4:4, 4:6, and 4:8, and the corresponding CTAB template concentrations were 0, 0.14, 0.27, 0.41 and 0.55 mol L^{-1}, respectively. The samples were marked with HPCs-1, HPCs-2, HPCs-3, HPCs-4 and HPCs-5, respectively. A solution of phenolic resin (PF) in ethanol as the source of carbon was added into the mixture with strong stirring. The mixture was left with a blending-layered-settlement program and dried in oven over night at 60 °C. After a two-step carbonization (200 °C for 2 h and 600 °C for 5 h) with a heating rate of 5 °C min^{-1}, the sample was cooled down to room temperature, etched with 3 M HCl thoroughly to remove $Ni(OH)_2$/NiO, then washed with deionized water and dried in oven at 100 °C. Finally, the resultant carbon was activated with 2 M HNO_3.

2.2. Physical characterization of the activated HPCs

The porous properties of the activated HPCs were examined by adsorption experiments of nitrogen, and adsorption/desorption isotherms of nitrogen were measured at 77 K on a Quantachrome autosorb automated gas sorption system. The estimation of the Brunauer–Emmett–Teller (BET) specific surface area (SSA), pore volume and pore size distribution (PSD) were carried out according to the Barrett–Joyner–Halenda (BJH).

2.3. Preparation of the activated HPCs electrodes

As usual in such devices, the supercapacitor electrodes materials are consisted of 80 wt% activated HPCs, 10 wt% acetylene black, and 10 wt% polyvinylidene fluoride (PVDF). After well mixed, the mixtures were blended to obtain slurries. Then the slurries were coated on nickel foams that were used as current collectors and dried in vacuum overnight at 353 K for 12 h. The geometric surface area of the electrodes was kept to be 1.0 cm^2.

2.4. Evaluation of the electrochemical properties

The electrochemical performances of the as-prepared electrode materials were characterized by cyclic voltammetry (CV) between −1.0 and 0 V with scan rates ranging from 1 to 20 mV s^{-1}, galvanostatic charge–discharge tests at various constant current densities with cutoff voltage of 0–1 V, electrochemical impedance spectroscopy (EIS) in the frequency range from 10^5 Hz to 10^{-2} Hz with amplitude of 5 mV, and self-discharging recording decline of cell voltage (1.0 V) over lengthy periods of time. The CV, the galvanostatic charge/discharge and EIS measurements were performed by means of electrochemical analyzer systems, CHI660 (CH Instruments, USA). The experiments of CV and EIS were carried out using a three-electrode system, in which a nickel sheet and the saturated calomel electrode via a luggin capillary with a salt bridge were used as counter and reference electrodes, respectively. And the galvanostatic charge/discharge measure was performed in a two-electrode configuration, in which the counter and reference electrodes are the same as the work electrode. The cycle life and self-discharging were measured by potentiostat/galvanostat (BTS 6.0, Neware, Guangdong, China) on button cell supercapacitors. The symmetrical button supercapacitors were assembled according to the order of electrode–separator–electrode. And all tests were measured in 6 M KOH electrolyte.

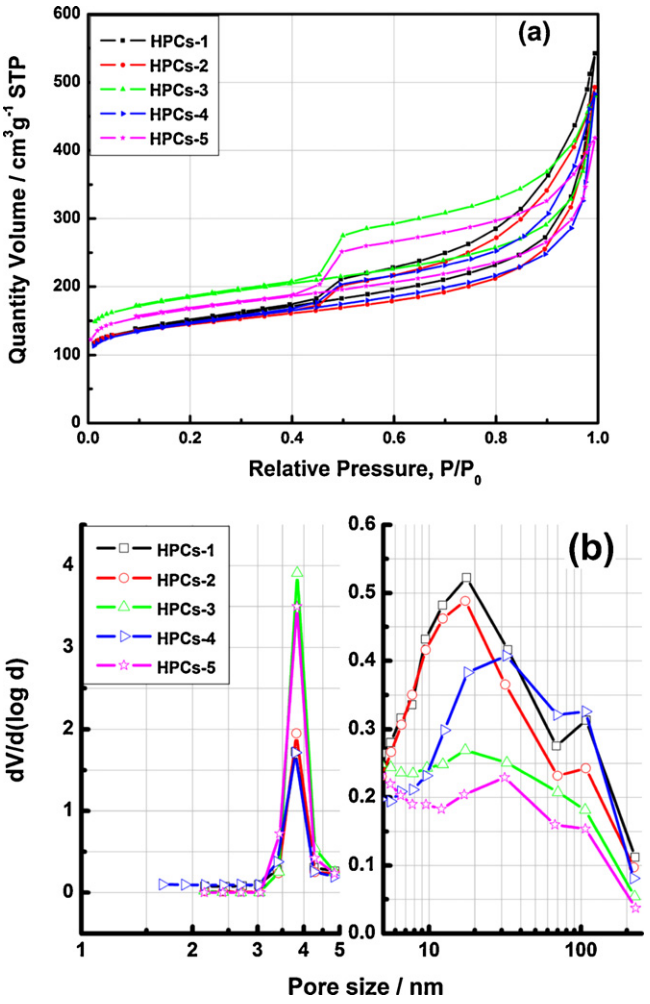

Fig. 1. (a) Nitrogen ads-desorption isotherms of the activated HPCs at 77 K. (b) The pore size distributions (BJH) of the activated HPCs.

3. Results and discussion

3.1. Structure analysis

The microstructures of activated hierarchically porous carbons are identified by nitrogen adsorption measurements. The nitrogen adsorption–desorption isotherms and pore size distribution curves of the activated HPCs marked with HPCs-1, HPCs-2, HPCs-3, HPCs-4 and HPCs-5 are shown in Fig. 1, respectively. As shown in Fig. 1(a), the nitrogen adsorption–desorption isotherms of the activated HPCs are close to IUPAC type-IV with capillary condensation steps and distinct hysteresis loops (type H4) [16] at relative pressures (P/P_0) higher than 0.4, which means the existence of mesopores. The isotherms increase gradually at relative pressure $P/P_0 < 0.01$, which indicates that all activated HPCs have micropores in this region. Furthermore, the isotherms rise sharply at relative pressure P/P_0 close to 1, which is the indicative of macropores. The micropore volume (V_{micro}) calculated by V–t method [17] is 0.13, 0.14, 0.19, 0.13 and 0.17 $cm^3\,g^{-1}$ for the activated

Table 1
Textural properties of the activated HPCs.

Activated HPCs	C_{CTAB} (mol L^{-1})	Ni:CTAB ratio	Surface area (m^2 g^{-1})		Pore size (nm)	Volume (cm^3 g^{-1})	
			S_{BET}	S_{micro}		V_{total}	V_{micro}
HPCs-1	0	4:0	546	300	3.80	0.75	0.13
HPCs-2	0.14	4:2	544	361	3.82	0.66	0.14
HPCs-3	0.27	4:4	689	462	3.84	0.61	0.19
HPCs-4	0.41	4:6	537	323	3.79	0.66	0.13
HPCs-5	0.55	4:8	615	405	3.83	0.57	0.17

HPCs-1, HPCs-2, HPCs-3, HPCs-4 and HPCs-5, respectively. The BET SSA, total pore volume and other textural properties of the activated HPCs are summarized in Table 1. It can be found that the BET SSA of the activated HPCs are 546, 544, 689, 537 and 615 m^2 g^{-1} for the activated HPCs-1, HPCs-2, HPCs-3, HPCs-4 and HPCs-5, respectively; whereas the total pore volume is 0.75, 0.66, 0.61, 0.66 and 0.57 cm^3 g^{-1} for the above materials. Apparently, when the concentration of CTAB < 0.27 mol L^{-1}, there are few mesopores existence in the materials; and when the concentration of CTAB > 0.27 mol L^{-1}, the mesopores in the materials may collapse and convert into macropores in the carbonization process. Thus, close observation of subsequent data reveals that the activated HPCs-3 (C_{CTAB} = 0.27 mol L^{-1}) has the largest specific surface areas and microporous volume than other activated HPCs. It may be probably attributed to the synergistic effect of dual-template when the concentration of CTAB = 0.27 mol L^{-1} (the molar ratio of two templates is about 4:4). Fig. 1(b) is the PSD curves of the activated HPCs which are determined by BJH method. All curves show similar mesopore distributions, and the pores size is between 3.79 and 3.84 nm with the variation of less than 2%. Comparatively, the activated HPCs-3 possesses the most mesopores among all the activated HPCs and a quantity of macropores.

3.2. Measurement of the electrochemical performance

Fig. 2(a) displays the cyclic voltammetries of the activated hierarchically porous carbon electrodes at the scan rate of 1 mV s^{-1} with the potential range (vs. Hg/HgO) between 0.0 V and −1.0 V in 6 M KOH electrolyte. All the voltammetric curves are close to rectangular shape, which indicates that the activated HPCs acting as EDLCs electrodes have excellent reversibility in aqueous electrolyte. Some slight deviation from rectangular shapes is due to the present of a remarked pseudo-capacitance. The capacitance values can be determined by Eq. (1) [18]:

$$Cs,t = \frac{Ia + |Ic|}{2W(dV/dt)} \quad (1)$$

where $C_{s,t}$, Ia, Ic, W and dV/dt are the specific capacitance (F g^{-1}), the current (A) of anodic and cathodic voltammetric curves on positive and negative sweeps, the mass of the material (g) (only including the mass of the activated HPCs, the same below), and the sweep rate (mV s^{-1}), respectively. The gravimetric specific capacitance (C_g) and surface capacitance (C_s, capacitance per unit surface area of carbon) of the activated HPCs electrodes at 1 mV s^{-1} calculated from Eq. (1) are listed in Table 2. The C_g is 270, 252, 272, 180 and 213 F g^{-1} for the activated HPCs-1, HPCs-2, HPCs-3, HPCs-4 and HPCs-5, respectively. With an increase in the surfactant template concentration from 0 mol L^{-1} to 0.55 mol L^{-1}, the specific capacitance decreased by 49%. Notwithstanding the activated HPCs-1 (C_{CTAB} = 0 mol L^{-1}) and HPCs-3 (C_{CTAB} = 0.27 mol L^{-1}) exhibit a higher specific capacitance than those of other carbons as the CTAB concentration changing; moreover, the activated HPCs-3 and HPCs-4 (C_{CTAB} = 0.41 mol L^{-1}) have superior retention of capacitance than those of others (Fig. 2(b)). Fig. 2(b) further demonstrates the comparisons of the specific capacitance values (evaluated by Eq. (1)) depending on scan rates (from 1 to 20 mV s^{-1}) and CTAB concentration (0–0.55 mol L^{-1}) for all the electrodes. It may be noted that even at higher scan rate of 20 mV s^{-1}, the activated HPCs-3 and HPCs-4 still have retention of more than 73%, indicating that the conductivity is high enough to assure good charge propagation. Consequently, the results obtained from CV show that the activated HPCs-3 performs excellent electrochemical reversible behavior.

High electrochemical stability can be characterized by galvanostatic charge/discharge for supercapacitors. Fig. 3 presents the charge/discharge curves of the activated HPCs-1, HPCs-2, HPCs-3, HPCs-4 and HPCs-5 as supercapacitors measured at the current densities of 1 A g^{-1} in 6 M KOH, respectively. The curves are almost symmetrical isosceles lines, demonstrating that the activated HPCs supercapacitors have typical porous carbon supercapacitive

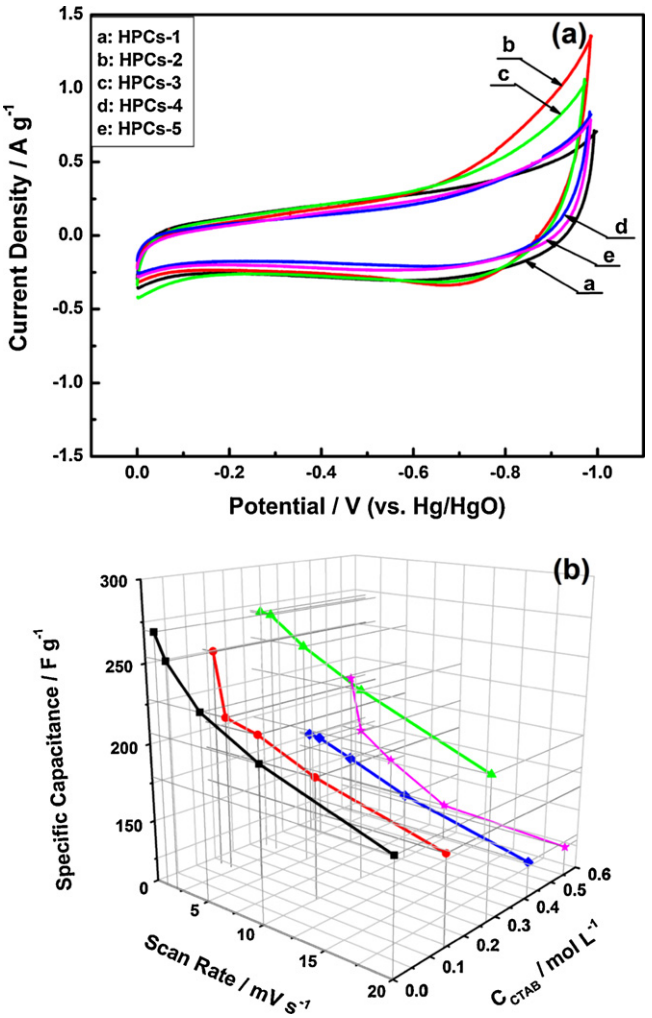

Fig. 2. (a) The CV curves of the activated HPCs electrodes at scan rate of 1 mV s^{-1}. (b) The specific capacitance (Z axis) of the porous carbon electrodes vs. scan rates (X axis) and CTAB concentration (Y axis).

Table 2
The comparison of supercapacitive property of the activated HPCs.

Activated HPCs	C_{CTAB} (mol L^{-1})	C_g[a] (F g^{-1})	C_s[a] (μF cm^{-2})	C[b] (F g^{-1})	IR drop (V)	R[c] (Ω)	R_s[d] (Ω)	C[e] (F g^{-1})
HPCs-1	0	270	49.5	58	0.02	2.29	1.22	168
HPCs-2	0.14	252	46.3	47	0.02	2.49	1.04	157
HPCs-3	0.27	272	39.5	60	0.01	1.98	1.08	210
HPCs-4	0.41	180	33.5	42	0.01	1.28	0.98	121
HPCs-5	0.55	213	34.6	43	0.03	2.84	1.09	140

[a] The capacitance of electrodes calculated from CV at the scan rate of 1 mV s^{-1}.
[b] The capacitance of supercapacitors calculated from cycle life at current density of 1 A g^{-1}.
[c] The inner resistance of supercapacitors tested by IR drop.
[d] The electrolyte resistance of supercapacitors tested by EIS.
[e] The capacitance of electrodes calculated from EIS at the frequency about 0.01 Hz.

behavior and stable electrochemical properties. And at the beginning of discharge there is a few sudden potential drop (IR drop) which is attributed to the resistance of electrolytes and the inner resistance of ion diffusion in micropore [19]. Usually, IR drop is a direct measure of equivalent series resistance (ESR) which influences the overall power performance of a capacitor. In order to clearly calculate the IR value, the inset in Fig. 3 depicts the IR drops of the activated HPCs-1 and HPCs-3. It can be found from Table 2 that the IR drops of the different activated HPCs are all very small value. Generally speaking, on the basis of the difference of supercapacitor capacitance (calculated by Eq. (2) [20]), the charge/discharge phases will maintain different time.

$$Cm = \frac{itd}{m\Delta V} \quad (2)$$

where C_m is the specific capacitance (F g^{-1}), i is the charge/discharge current (A), ΔV is the potential range of the charge/discharge (V), t_d is the discharge time (s), and m is the mass of active material (g) within the electrode. In Fig. 3, the activated HPCs-1 and HPCs-3 keep nearly same discharging time, but the activated HPCs-3 exhibits lower IR drop (showed in Fig. 3, insert). Based on the calculating results from Fig. 3, the specific capacitances of the activated HPCs-1, HPCs-2, HPCs-3, HPCs-4 and HPCs-5 at 1 A g^{-1} are about 60, 49, 61, 44 and 45 F g^{-1}, respectively. Moreover, the charge/discharge efficiencies of the different activated HPCs supercapacitors are all close to 100%. Above results indicate that a high charge/discharge propagation, low resistivity and good reversible process can be expected on the activated HPCs electrodes [21]. Especially, the activated HPCs-3 performs excellent charging/discharging electrochemical property and lower IR drop.

Long cycle life of supercapacitors is paramount evaluation for practical applications. Fig. 4 reveals the change of specific capacitance versus cycle number for the activated HPCs at the constant current charge/discharge density of 1 A g^{-1}. After 5000 consecutive cycles, the specific capacitance still keep at 58, 47, 60, 42 and 43 F g^{-1} for the activated HPCs-1, HPCs-2, HPCs-3, HPCs-4 and HPCs-5, respectively. These data illustrate that the supercapacitors using the activated HPCs as electrode active materials present all good cycling stability in the repetitive charge/discharge cycling. Particularly, the supercapacitor using the activated HPCs-3 as electrode active material exhibits excellent cyclic stability.

Impedance spectroscopy (EIS) is commonly used to analyze the electrochemical properties of supercapacitors about characteristic frequency responses. Fig. 5(a) shows the ac impedance spectrum (Nyquist plots) and Fig. 5(b) presents capacitance responding to the frequency for electrodes of the activated HPCs-1, HPCs-2, HPCs-3, HPCs-4 and HPCs-5, respectively. The impedance is measured versus Hg/HgO reference electrode. It can be found in Fig. 5(a) that there are straight lines in the low-frequency region (lower than 100 Hz) because of Warburg impedance. The straight line part leans more towards the imaginary axis, which indicates a good capacitive behavior. Furthermore, the impedance in high frequency (Fig. 5(a), inset) has a special arc-shaped curve that means the microstructures of orbicular pores [22]. Electrolyte resistance (R_S) listed in Table 2 is estimated around 1.22, 1.04, 1.08, 0.98 and 1.09 Ohm for each activated HPCs electrodes from the crossover point of the highest frequency with the real part of the impedance. Charge-transfer resistance is extremely low from the inconspicuous

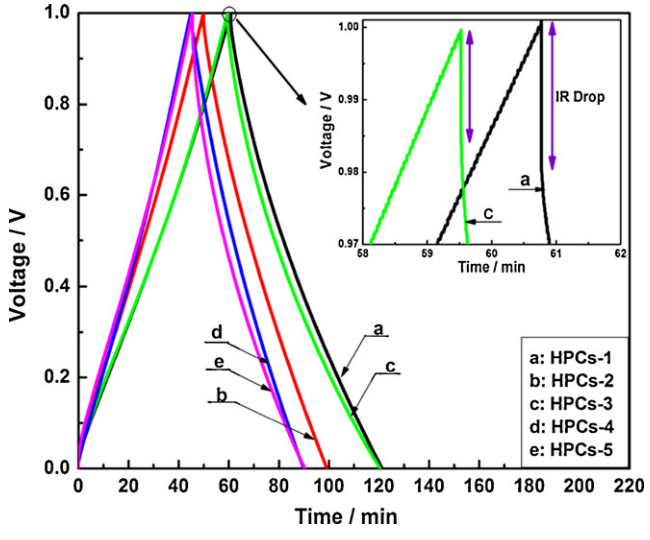

Fig. 3. The galvanostatic charging-discharging curves of the activated HPCs supercapacitors at 1 A g^{-1}, and IR drop of the activated HPCs-1, HPCs-3 insert.

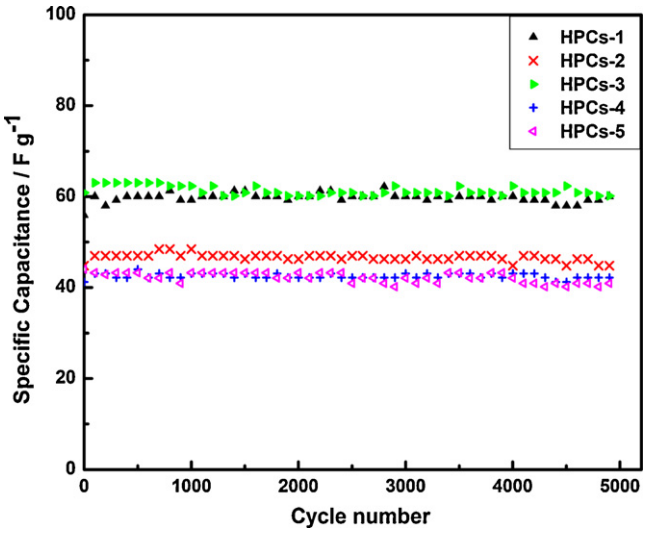

Fig. 4. The cycle life (5000 times) of the activated HPCs at current density of 1 A g^{-1}.

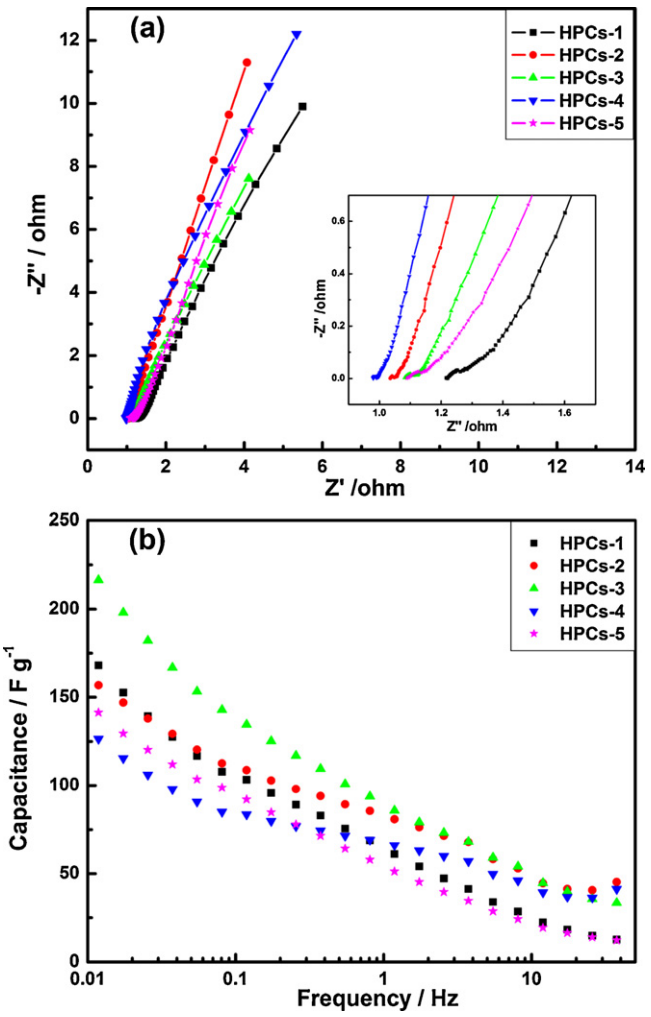

Fig. 5. (a) Nyquist plot based on activated HPCs electrodes with the frequency range of 10^5 to 10^{-2} Hz (the inset shows the expanded high-frequency region of the plot). (b) Imaginary part of the capacitance with the frequency for activated HPCs electrode.

semicircle for the activated HPCs electrodes (Fig. 5(a), insert). The specific capacitances of the activated HPCs electrodes responding frequencies are calculated from Eq. (3) [23], and the results are given in Fig. 5(b).

$$Cm = -\frac{1}{2\pi f Z''} \tag{3}$$

where C_m is the equivalent series capacitance ($F\,g^{-1}$), f is the frequency (Hz), Z'' (ohm) is the imaginary part in impedance. As the change of CTAB concentration, the activated HPCs-3 electrodes obtains the highest specific capacitance of 210 $F\,g^{-1}$ at low frequency range approximately to 0.01 Hz and has better electrochemical performance than the rest of activated HPCs due to the optimal microstructure. However, in the high frequency over 1000 Hz all the electrodes cannot display capacitive behavior because of the ionic mobility.

3.3. The effects of CTAB concentration on self-discharging of supercapacitor

After being charged, the supercapacitors are in a state of high Gibbs energy which is relation to their discharged states; and there is a thermodynamic "driving force" for their self-discharge on open-circuit [24,25]. The self-discharge behavior of supercapacitors is an important factor when considering their suitability for some applications. In previous articles [26,27], there are three main distinguishable self-discharge mechanisms are discussed by Conway models [24,28]. The three main models are listed as follows:

I: An activation-controlled Faradaic process. Here the decline of voltage (V or V_t) versus log time ($\log t$) would give a straight line:

$$V = -\frac{RT}{\alpha F}\ln\left[\frac{\alpha i0}{RTC}\right] - \frac{RT}{\alpha F}\ln\left(t + \frac{C\tau}{i0}\right) \tag{4}$$

$$\text{Simply} \quad Vt = Vi - A\log(t+\tau) \tag{5}$$

where V is the supercapacitors voltage (V) during the self-discharging, R is the universal gas constant (8.314 $J\,K^{-1}\,mol^{-1}$), T is the temperature (298 K) of the system, α is the transfer coefficient, F is the faraday constant (96,500 $C\,mol^{-1}$), i_0 is the exchange current density ($A\,cm^{-2}$), C is the capacitance ($F\,g^{-1}$), t is the self-discharging time (s), τ is an integration constant, V_i is the initial charging potential (V) and A is a constant related to the Tafel slope $RT/\alpha F$ [28]. This model involves the 'over charging' Faradaic reaction of a species which is either at high concentration in the cell or is confined to the surface.

II: A diffusion controlled Faradaic process. Here the decline of voltage (V) vs. the square root of t ($t^{1/2}$) would give a straight line:

$$Vt = Vi - \frac{2zFAD^{1/2}\pi^{1/2}c_0}{C}t^{1/2} \tag{6}$$

$$\text{Simply} \quad V = V0 - m\sqrt{t} \tag{7}$$

where z is the charge (C), A is the electro-active area (cm^2), D is the diffuse coefficient ($m^2\,s^{-1}$) of the redox species, c_0 is the initial concentration ($mol\,L^{-1}$), and m is diffuse parameter ($V\,s^{-1/2}$). This model is based on the Faradaic reaction of a species which has a low concentration in the EC and the reaction of the electrode surface relying on diffusing transport.

III: An internal ohmic leakage or a 'short circuit' due to faulty construction. Here a plot of ln voltage ($\ln V$) versus time (t) would give a linear relationship:

$$V = V0\exp\left[\frac{-t}{RLC}\right] \tag{8}$$

where R_L is the resistance (ohm) of the ohmic contact, C is the capacitance ($F\,g^{-1}$) of the supercapacitors and R_LC is the time constant (h). This model describes two adjacent electrodes through a load in improperly sealed bipolar cell designs [24].

Although the self-discharging process is complex and difficult to understand, it can be analyzed simply by using above models. In this paper, after 5000 times constant charging–discharging cycles, the self-discharge profiles of the activated HPCs-1, HPCs-2, HPCs-3, HPCs-4 and HPCs-5 are examined with 6 M KOH electrolytes when the supercapacitors are charged from 0 V to 1.0 V. In Fig. 6(a), the supercapacitors with the activated HPCs materials show a significant self-discharge after they are fully charged to their rated voltage 1.0 V. It can be seen that there is no striking difference in the self-discharge profile until the concentration of CTAB reaches 0.55 $mol\,L^{-1}$ which is marked with activated HPCs-5. According to above three self-discharge mechanisms, Fig. 6(b) shows the self-discharge profile of the supercapacitors of the activated HPCs charged to 1.0 V plotted the decline of voltage versus log time for the first 10 min; Fig. 6(c) reveals the self-discharge profile plotted the decline of voltage versus time$^{1/2}$ for the next 420 min; and Fig. 6(d) presents that during self-discharge process of the activated HPCs, the voltage appears to decay exponentially after about 420 min. Meanwhile, the measured data (the straight lines) and linear fitted data (scatters of points) are indicated in the Fig. 6(b–d). Apparently, it can be found that the activation-controlled Faradaic process dominates the self-discharging for the first 10 min (Fig. 6(b)), where there is a linear relation (voltage vs.

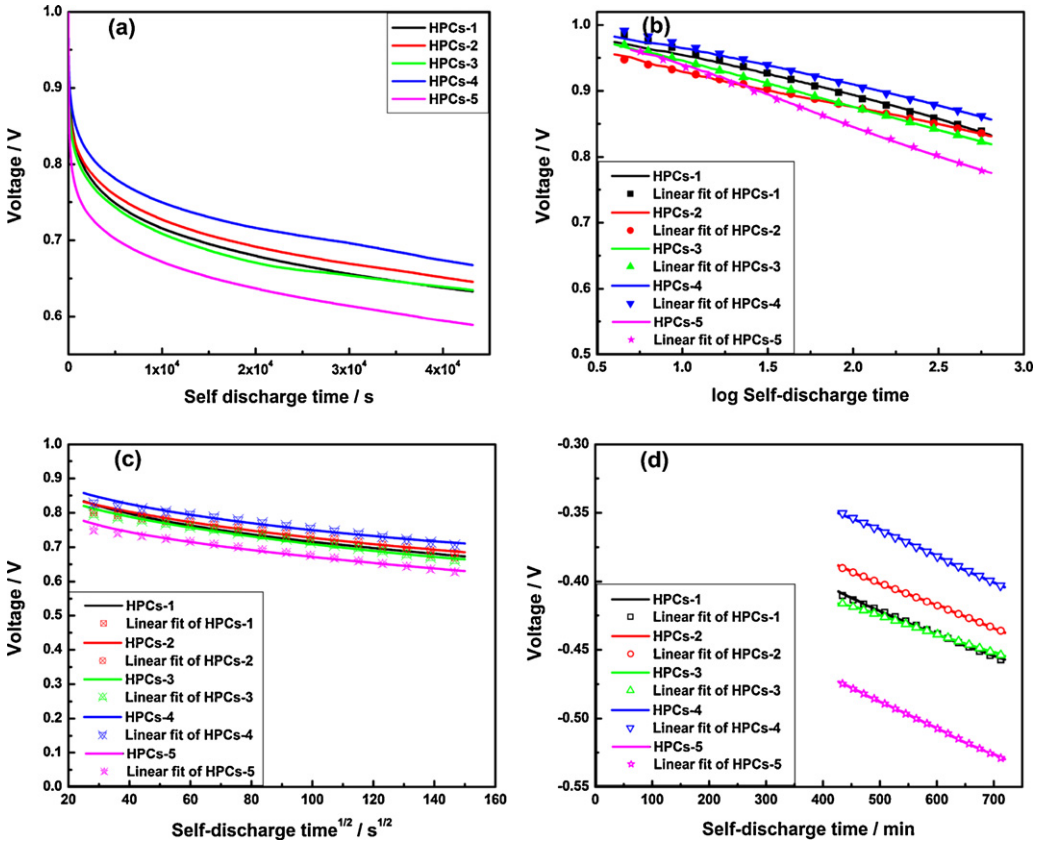

Fig. 6. Self-discharge profile of the activated HPCs supercapacitors charged to 1.0 V, plotted by (a) voltage vs. time; (b) voltage vs. log time for the first 10 min; (c) voltage vs. time$^{1/2}$ for the next 420 min; (d) voltage to decay exponentially versus time after 420 min. Measured data (lines) and linear fitted data (scatters of points) for figures of b–d.

log t). However, the diffusion-controlled process maintains the self-discharging for the next 420 min, where there is a linear relation (voltage vs. $t^{1/2}$) (Fig. 6(c)). Moreover, after 420 min the internal ohmic leakage is the primary factor to cause the voltage to decay exponentially (ln V vs. t) (Fig. 6 (d)).

Consequently, the mechanisms of self-discharge process for all activated HPCs are consisted of three sections. When $0 \le t \le 10$ min, the self-discharge process is in agreement with activation-controlled Faradaic process; when $10 \le t \le 420$ min, the self-discharge process is a diffusion-controlled process; and when $420 \le t \le 720$ min, the self-discharge process becomes an ohmic leakage process.

4. Conclusions

Various activated HPCs electrode materials are prepared by self-assembly process via adjusting surfactant concentration of 0–0.55 mol L^{-1}. It can be identified that the concentration of CTAB has an important impact on the specific surface area and pore size of sample. All of the synthesized activated HPCs have large specific surface area and wide pore-size distribution. The mechanisms of self-discharge process for all activated HPCs are consisted of three sections including activation-controlled Faradaic process, diffusion-controlled process and ohmic leakage process. In addition, all activated HPCs present remarkable supercapacitive behaviors, long cycle life, small ohmic resistance and low self-discharging. Particularly, the activated HPCs-3 prepared at C_{CTAB} = 0.27 mol L^{-1} shows the largest BET specific surface area of 689 m^2 g^{-1} and the pore size of 3.84 nm, which result in the optimum electrode capacitance of 272 F g^{-1} at the scan rate of 1 mV s^{-1} and supercapacitor capacitance of 61 F g^{-1} at the current density of 1 A g^{-1} as well as the low IR drop of 0.01 V and electrolyte resistance of 1.08 Ω. Therefore, it can be concluded that the activated HPCs-3 might be a promising choice for preparing high performance supercapacitor.

Acknowledgements

This work was financially supported by the National Natural Science Foundation of China (Grant No. 51072173), Specialized Research Fund for the Doctoral Program of Higher Education (Grant No. 20094301110005).

References

[1] E. Frackowiak, F. Béguin, Carbon 39 (2001) 937–950.
[2] S. Wen, M. Jung, O. Joo, S. Mho, Curr. Appl. Phys. 6 (2006) 1012–1015.
[3] T. Bordjiba, M. Mohamedi, L.H. Dao, Adv. Mater. 20 (2008) 815–819.
[4] J. Chmiola, G. Yushin, R. Dash, Y. Gogotsi, J. Power Sources 158 (2006) 765–772.
[5] M. Sevilla, S. Álvarez, T.A. Centeno, A.B. Fuertes, F. Stoeckli, Electrochim. Acta 52 (2007) 3207–3215.
[6] Y.L. Cao, J.M. Cao, M.B. Zheng, J.S. Liu, G.B. Ji, J. Solid State Chem. 180 (2007) 792–798.
[7] L. Chen, R.K. Singh, P. Webley, Microp. Mesop. Mater. 102 (2007) 159–170.
[8] L.H. Kao, T.C. Hsu, Mater. Lett. 62 (2008) 695–698.
[9] J. Górka, M. Jaroniec, Carbon 49 (2011) 154–160.
[10] W. Xing, S.Z. Qiao, R.G. Ding, F. Li, G.Q. Lu, Z.F. Yan, H.M. Cheng, Carbon 44 (2006) 216–224.
[11] S.L. Orozco, A. Inayat, A. Schwab, T. Selvam, W. Schwieger, Adv. Mater. 23 (2011) 2602–2615.
[12] B. Zhao, M.M. Collinson, Chem Mater. 22 (2010) 4312–4319.
[13] A.R. Studart, J. Studer, L. Xu, K. Yoon, H.C. Shum, D.A. Weitz, Langmuir 27 (2011) 955–964.
[14] D.W. Wang, F. Li, M. Liu, G.Q. Lu, H.M. Cheng, Angew. Chem. Int. Ed. 47 (2008) 373–376.
[15] D.R. Rolison, Science 299 (2003) 1698–1701.
[16] F. Rojas, I. Kornhauser, C. Felipe, J.M. Esparza, S. Cordero, A. DomÍnguez, J.L. Riccardo, Phys. Chem. Chem. Phys. 4 (2002) 2346–2355.
[17] G. Halsey, J. Chem. Phys. 16 (1948) 931–937.

[18] C.C. Hu, C.C. Wang, Electrochem. Commun. 4 (2002) 554–559.
[19] H. Teng, Y.J. Chang, C.T. Hsieh, Carbon 39 (2001) 1981–1987.
[20] Y.G. Wang, H.Q. Li, Y.Y. Xia, Adv. Mater. 18 (2006) 2619–2623.
[21] S. Mitani, S.I. Lee, K. Saito, Y. Korai, I. Mochida, Electrochimi. Acta 51 (2006) 5487–5493.
[22] H. Keiser, K.D. Beccu, M.A. Gutjahr, Electrochim. Acta 21 (1976) 539–543.
[23] K.S. Ryu, Y.G. Lee, K.M. Kim, Y.J. Park, Y.S. Hong, X.L. Wu, M.G. Kang, N.G. Park, R.Y. Song, J.M. Ko, Synth. Met. 153 (2005) 89–92.
[24] J.J. Niu, B.E. Conway, W.G. Pell, J. Power Sources 135 (2004) 332–343.
[25] J. Kowal, E. Avaroglu, F. Chamekh, A. Šenfelds, T. Thien, D. Wijaya, D.U. Sauer, J. Power Sources 196 (2011) 573–579.
[26] J. Black, H.A. Andreas, J. Power Sources 195 (2010) 929–935.
[27] J. Black, H.A. Andreas, Electrochim. Acta 54 (2009) 3568–3574.
[28] B.E. Conway, W.G. Pell, T.C. Liu, J. Power Sources 65 (1997) 53–59.